NASA/TM-20210024128

Lunar Simulant Deposition Technique for Dust Tolerance Studies

Stephen Gerdts, Nathan Jimenez, and Patrick H. Dunlap, Jr.
Glenn Research Center, Cleveland, Ohio

January 2022

NASA STI Program . . . in Profile

Since its founding, NASA has been dedicated to the advancement of aeronautics and space science. The NASA Scientific and Technical Information (STI) Program plays a key part in helping NASA maintain this important role.

The NASA STI Program operates under the auspices of the Agency Chief Information Officer. It collects, organizes, provides for archiving, and disseminates NASA's STI. The NASA STI Program provides access to the NASA Technical Report Server—Registered (NTRS Reg) and NASA Technical Report Server—Public (NTRS) thus providing one of the largest collections of aeronautical and space science STI in the world. Results are published in both non-NASA channels and by NASA in the NASA STI Report Series, which includes the following report types:

- TECHNICAL PUBLICATION. Reports of completed research or a major significant phase of research that present the results of NASA programs and include extensive data or theoretical analysis. Includes compilations of significant scientific and technical data and information deemed to be of continuing reference value. NASA counter-part of peer-reviewed formal professional papers, but has less stringent limitations on manuscript length and extent of graphic presentations.

- TECHNICAL MEMORANDUM. Scientific and technical findings that are preliminary or of specialized interest, e.g., "quick-release" reports, working papers, and bibliographies that contain minimal annotation. Does not contain extensive analysis.

- CONTRACTOR REPORT. Scientific and technical findings by NASA-sponsored contractors and grantees.

- CONFERENCE PUBLICATION. Collected papers from scientific and technical conferences, symposia, seminars, or other meetings sponsored or co-sponsored by NASA.

- SPECIAL PUBLICATION. Scientific, technical, or historical information from NASA programs, projects, and missions, often concerned with subjects having substantial public interest.

- TECHNICAL TRANSLATION. English-language translations of foreign scientific and technical material pertinent to NASA's mission.

For more information about the NASA STI program, see the following:

- Access the NASA STI program home page at http://www.sti.nasa.gov

- E-mail your question to help@sti.nasa.gov

- Fax your question to the NASA STI Information Desk at 757-864-6500

- Telephone the NASA STI Information Desk at 757-864-9658

- Write to:
  NASA STI Program
  Mail Stop 148
  NASA Langley Research Center
  Hampton, VA 23681-2199

NASA/TM-20210024128

Lunar Simulant Deposition Technique for Dust Tolerance Studies

Stephen Gerdts, Nathan Jimenez, and Patrick H. Dunlap, Jr.
Glenn Research Center, Cleveland, Ohio

National Aeronautics and
Space Administration

Glenn Research Center
Cleveland, Ohio 44135

January 2022

Acknowledgments

The authors would like to acknowledge NASA's Human Landing System (HLS) Advanced Development Office for supporting this effort and providing the funding that enabled development of the Uniform Dust Deposition System, as well as Janice Mather and Heather Oravec for their technical contributions.

Level of Review: This material has been technically reviewed by technical management.

Available from

NASA STI Program
Mail Stop 148
NASA Langley Research Center
Hampton, VA 23681-2199

National Technical Information Service
5285 Port Royal Road
Springfield, VA 22161
703-605-6000

This report is available in electronic form at http://www.sti.nasa.gov/ and http://ntrs.nasa.gov/

Lunar Simulant Deposition Technique for Dust Tolerance Studies

Stephen Gerdts, Nathan Jimenez, and Patrick H. Dunlap, Jr.
National Aeronautics and Space Administration
Glenn Research Center
Cleveland, Ohio 44135

Summary

A renewed interest in lunar exploration has spawned an array of development efforts for lunar surface assets. These systems depend on the reliable operation of mechanisms and components that may be susceptible to performance degradations or failure due to dust. The Uniform Dust Deposition System was developed at the NASA Glenn Research Center to provide repeatable, uniform, and automated deposition of simulants on surfaces of interest for dust mitigation testing. The system is capable of depositing simulants on test articles up to 60 cm in diameter and 15 cm high in a dry air environment with less than 1 percent relative humidity while keeping users safe from aerosolized dust. The automation of the system allows for high testing throughput while not sacrificing test quality and allows the user to reduce data in parallel. The additional development of a simulant preparation technique complements the repeatability of the deposition physics during testing. The system includes an imaging subsystem that leverages the power of machine learning to count simulant particles and measure their size, thereby allowing for accurate predictions of surface deposition densities (coefficient of determination $R^2 = 0.93$) from images alone. The coverage of dust on a surface was shown to be uniform (coefficient of variation $CV < 0.11$), allowing developers to accurately evaluate the performance of their technology with a prescribed amount of lunar simulant, information that can be used to develop and refine models. The accuracy of the system is currently less than desired for a single deposition run, with a standard deviation (SD) ranging from 18 to 24 mg, or 0.839 to 1.184 mg/cm^2, for a 5-cm-diameter area. However, the accuracy can be improved by performing multiple deposition runs to build dust to a desired level. Testing has shown that a SD of 0.2 to 0.6 mg, or 0.076 to 0.227 mg/cm^2, can be achieved for a 5-cm-diameter area using this technique.

Acronyms

3D	three-dimensional
ASTM	American Society for Testing and Materials
CLPS	Commercial Lunar Payload Services
CONOPS	concept of operations
CV	coefficient of variation
DC	direct current
HEPA	high-efficiency particulate air
HLS	Human Landing System
IMU	inertial measurement unit
LDAB	lunar dust adhesion bell jar
NEMA	National Electrical Manufacturers Association
OSHA	Occupational Safety and Health Administration
PSD	particle size distribution
RH	relative humidity
SD	standard deviation
UDDS	Uniform Dust Deposition System

Introduction

A renewed interest in lunar exploration was initiated by the signing of Space Policy Directive–1 in December 2017 (Ref. 1). The directive calls for NASA to lead an innovative and sustainable exploration program with commercial and international partners, and it helped lay the foundation for the Artemis program, which will send the first woman and the next man to the surface of the Moon. The Artemis program, along with the Human Landing System (HLS) and Commercial Lunar Payload Services (CLPS) programs, has spawned an array of development efforts for lunar surface assets. These assets range from human-rated and robotic landers to autonomous mobile explorers and deployable towers. These systems all depend on the reliable operation of their mechanisms and components, which may be susceptible to performance degradations or failure due to dust.

Lunar dust has been described as “one of our greatest inhibitors to a nominal operation on the Moon” (Ref. 2). This is because lunar dust has abrasive and electrostatic properties that can disrupt systems in various ways (Ref. 3). Meteorites impact the Moon constantly, fracturing rocks into fine particles called regolith that coat the top 4 m of the Moon’s surface (Ref. 4). The lack of atmosphere and geological transport mechanisms (e.g., wind and rivers) on the Moon means that there is no process to reduce the roughness of these particles, leaving them extremely angular and abrasive (Ref. 5). An additional aspect to the challenge of lunar dust is the electrostatic charging of these particles due to interactions with the local plasma environment and solar electromagnetic radiation (Ref. 6). This results in the regolith becoming electrostatically attracted to surfaces of the opposite charge, making it very difficult to remove (Ref. 7). These conditions can cause the regolith to obscure optical systems, create extreme wear on astronauts’ spacesuits, disrupt mechanisms and rotary systems, and compromise the critical seals needed for habitable volumes and effective environmental control and life support systems (Ref. 8). The need to develop technology that can not only tolerate dust but thrive in its presence is critical for the establishment of sustainable architectures both on the Moon and at destinations farther into the solar system.

These risks associated with lunar dust were recognized as a top concern by NASA. As a result, NASA established a dust mitigation working group consisting of stakeholders and technology developers to work together to generate solutions for this problem (Ref. 9). One of the issues the group identified was the difficulty in performing tests in a repeatable fashion when evaluating the effect of lunar dust on systems. Measures taken to standardize the testing of dust include NASA Technical Standards such as “Classifications and Requirements for Testing Systems and Hardware to be Exposed to Dust in Planetary Environments” (Ref. 10), but uniformity remains a challenge. Dust is often applied to mechanisms or target surfaces in a much less controlled manner, using spoons, for example, or sprinkling it on by hand. Although these methods fulfill the requirement of contaminating a specimen, the amount of regolith deposited is often not measured, uniform, or repeatable. The creation of a system that can deposit a known amount of simulant per unit area at a known size fraction would create a reliable and standardized approach for testing a vast array of mechanisms across the industry. The development and validation of such a system is the focus of this paper.

The Uniform Dust Deposition System (UDDS) was developed with the aim of producing not only a system but a series of techniques for depositing and characterizing dust simulant for stakeholders to have available for use in testing. One such technique outlined in this paper is the preprocessing of the simulant for testing. Simulant preparation is instrumental for deposition uniformity due to the sensitivity of deposition physics to initial conditions. Once prepared, the simulant is loaded into the UDDS on a vibration plate that is then agitated using an electric motor by spinning an eccentric mass. The resulting deposition is a uniform column of particles of selectable size fraction that settles onto a desired target.

The system then transfers the target to an inspection area where images of the surface are taken with a microscope to characterize the amount of simulant deposited. The analysis is completed using a trained machine learning algorithm that recognizes particles, counts them, and feeds back a percent coverage. The entire process occurs within a glovebox filled with dry air at a relative humidity (RH) of less than 1 percent. Furthermore, all components were designed such that the whole system could be introduced and operated in a vacuum chamber to better represent the lunar environment. This paper outlines how the accuracy and precision of this system were evaluated through validation and verification testing.

System Requirements

Testing with lunar regolith simulants can be a difficult task to undertake given the stochastic nature of granular physics. Many factors contributed to the system's design requirements to produce a reliable, repeatable, and safe technique for depositing dust. The main factors included accuracy of the deposition, uniformity of the deposition, particle size distribution (PSD), imaging resolution, RH, operators' working environment, and throughput of test articles.

Accuracy of deposition was the first critical design requirement for the UDDS. The desired accuracy for the system was based on previous research conducted by Oravec et al., which determined that for size 2-309 silicone O-rings (S0383-70) the critical mass of dust contamination was 6.3 mg (≈1.5 mg/cm^2) (Ref. 11). With the contamination-to-failure levels for seals being so low, this seemed an appropriate target for a system that needed to have a very high level of accuracy, so the UDDS deposition accuracy requirement was set at 1.5 mg/cm^2. This high accuracy is also critical for solar panel and thermal radiator testing because their performance degradation is a function of contamination level (Ref. 12).

With such sensitive systems to test, not only is the accuracy of the deposition important, but also how uniformly the dust mass is distributed on the target surface. Uniformity of deposition on the target surface was thus the second critical design requirement for the UDDS. For the test data to be of use to researchers, a dusted surface needs to have a uniform layer of dust of a known PSD at a known concentration. For example, if tests are being performed to determine the contamination level at which a seal will fail, it is important for the entire circumference of the seal to have the same deposition concentration. This ensures there are no artificially high areas of contamination that will cause a seal to fail prematurely. To capture this need into a verifiable requirement, images must be collected at several locations on the contaminated surface during testing. Each image is analyzed for the percent coverage, and the coefficient of variation (CV) for the collection of images must be less than 20 percent. This allows for the assurance of uniformity across a range of deposition density levels, as each yields different percent coverages (i.e., higher density results in higher percent coverage but also the chance for variability).

To produce a deposition with an accurate PSD, the system would need to incorporate standard sieves procured from a manufacturer with a certificate of accuracy. The PSD can then be varied by switching out the standard sieves, as they contain varying mesh sizes; however, the sieves themselves do not control the PSD being deposited. They are used in conjunction with preprocessing and presieving of the simulant to deliver the desired PSD. For example, if the desired PSD range is 150 to 250 μm, the simulant cannot simply be placed in a No. 60 sieve, because the resulting deposition would also include all particle sizes below 250 μm. Instead, the simulant must be presieved, first by using a No. 60 sieve to remove the particles larger than 250 μm, then by using the No. 100 sieve to remove all particles smaller than 150 μm. The preprocessed simulant is placed into a No. 60 sieve when testing, ensuring all particles can pass through. To quantify the PSD of deposition on the target surface, a requirement for the imaging resolution was needed. The imaging requirement for the UDDS was a resolution of 10 μm with at least 100 pixels.

While considering requirements, the design of NASA's lunar dust adhesion bell jar (LDAB) system was explored. The primary design criterion of the LDAB system was to emulate the lunar environment thermally, atmospherically, and electrostatically (Ref. 13). Based on the review, a decision was made to design a system with components compatible with a 10^{-6} torr vacuum, like the LDAB, but the system would deposit simulants in dry air over a much larger area. Dry air is critical to a lunar dust testing environment because simulant can absorb moisture out of the air, a scenario not present on the Moon. Moisture in the simulant can then cause the finer sieved particles to clump together after passing through a sieve while being deposited on a surface. This can cause an artificially large particle to form on the surface and can affect the quality of the tests (Ref. 14). To mitigate this phenomenon, it was decided that the simulant would be desiccated prior to use, and dry air at less than 1 percent RH would be pumped into the glovebox before testing to purge the system.

The final requirements considered were operational ones related to human safety and throughput maximization. To comply with NASA and Occupational Safety and Health Administration (OSHA) standards for airborne silica, it was decided that the deposition would occur inside a commercially available glovebox (MBraun UNIlab pro model). This eliminated the need for an operator to wear a respirator and had the added benefit of keeping the laboratory space free from lunar simulant contamination. As for throughput, the target test time was set to 30 min to allow for multiple depositions in one workday. Automation ensured the system would be available for numerous test campaigns as well as ensuring repeatability from test to test. The requirements of the UDDS in its current form are summarized in Table I.

System Design

The UDDS is separated into three major subsystems: the deposition subsystem, the transfer subsystem, and the imaging subsystem (Figure 1). The deposition subsystem is where the deposition sieves are mounted along with the eccentric mass motor that generates the vibration. The transfer subsystem consists of an automated spinning plate, which sits on a mechanized rail system that allows for repeatable positioning of the target surface. Finally, the imaging subsystem houses the microscope and a remotely controlled camera mounted on a rail with a motorized focus stage. Together these subsystems function automatically to ensure quick and repeatable tests.

TABLE I.—SUMMARY OF REQUIREMENTS

Requirement	Specification
Deposition level accuracy	±1.5 mg/cm^2
Deposition uniformity	<20 percent coefficient of variation (CV) of percent of area covered
Deposition surface size	60-cm (24-in.) diameter
Test article height	15 cm (6 in.)
Atmosphere	<1 percent relative humidity
Vacuum (material compatibility)	10^{-6} torr
Exposure control	Glovebox
Deposition test time	<30 min
Simulant size fraction range	20 to 1,000 µm
Image resolution (minimum particle size)	10 µm
Temperatures	Room temperature (evolvable with heaters and cold plates)

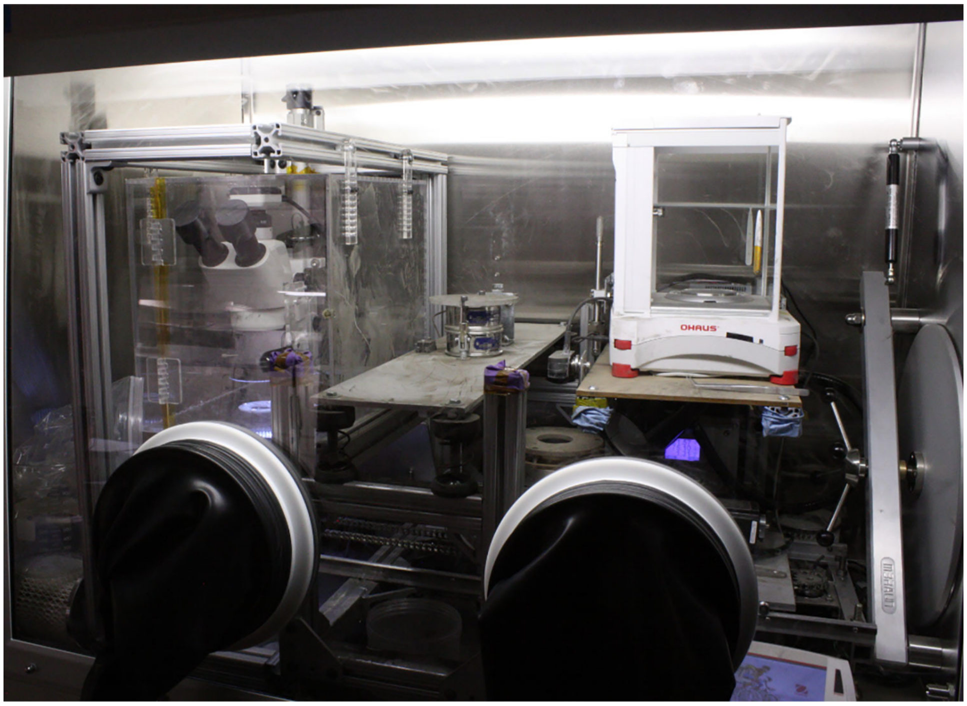

Figure 1.—Entire system inside glovebox.

Deposition Subsystem

The deposition subsystem is the backbone of the UDDS (Figure 2). It was sized to maximize the target surface that could fit within the existing glovebox (60-cm diameter × 15-cm height), although its size can be modified to fit inside other gloveboxes or vacuum chambers. The system consists of a frame that supports a vibration plate via four spring mounts, two standard sieves with a dust trap, and an eccentric mass motor. All components of the deposition subsystem are made of vacuum-compatible materials such as aluminum, 304 stainless steel, and 18-8 stainless steel.

The spring mounts rest on an adjustable portion of the frame (Figure 2) and allow the vibration plate to be agitated in isolation. The adjustability of the frame allows the operator to select different deposition heights or accommodate larger fixturing. The stiffness of these spring mounts was selected by summing the total mass of the vibration plate, sieves, motor, and hardware and dividing by the number of spring mounts desired. The spring mounts with the closest load capacity were selected, resulting in an underdamped system. The vibration plate holds two standard 7.6-cm (3-in.) sieves that hold the simulant for deposition.

A two-sieve architecture was adopted to improve the deposition uniformity and control the deposition rate. Both sieves are installed with the same mesh size to ensure all particles can pass through. As noted earlier, the vibration plate accepts 7.6-cm (3-in.) standard sieves that can be quickly switched out. A mounting hole at the center of the vibration plate seats the sieves. Two swing bolts tighten down a clamping plate that goes over the two sieves to fix them in place.

Another component mounted on the vibration plate is the eccentric mass motor and its mounting bracket. The motor is mounted such that the axis of rotation is normal to the top surface of the vibration plate, creating a circular horizontal movement (Figure 3). Its bracket sits 12 cm from the center of the plate. For lower deposition rates or larger PSDs, just one motor is used. For faster deposition rates or smaller PSDs, the vibration plate is designed to accept another motor that would be mounted on the opposite side of the sieves. When both motors are installed, they should be installed with their axes of rotation at 45° to the vibration plate and opposite each other. This creates an agitation motion that moves the simulant particles both up and down and in a circular motion within the sieves. This improves the flow rate of the particles through the sieves, as fewer large particles would get caught in the openings of the sieve's mesh. This is especially true for finer PSD depositions (≈20 µm).

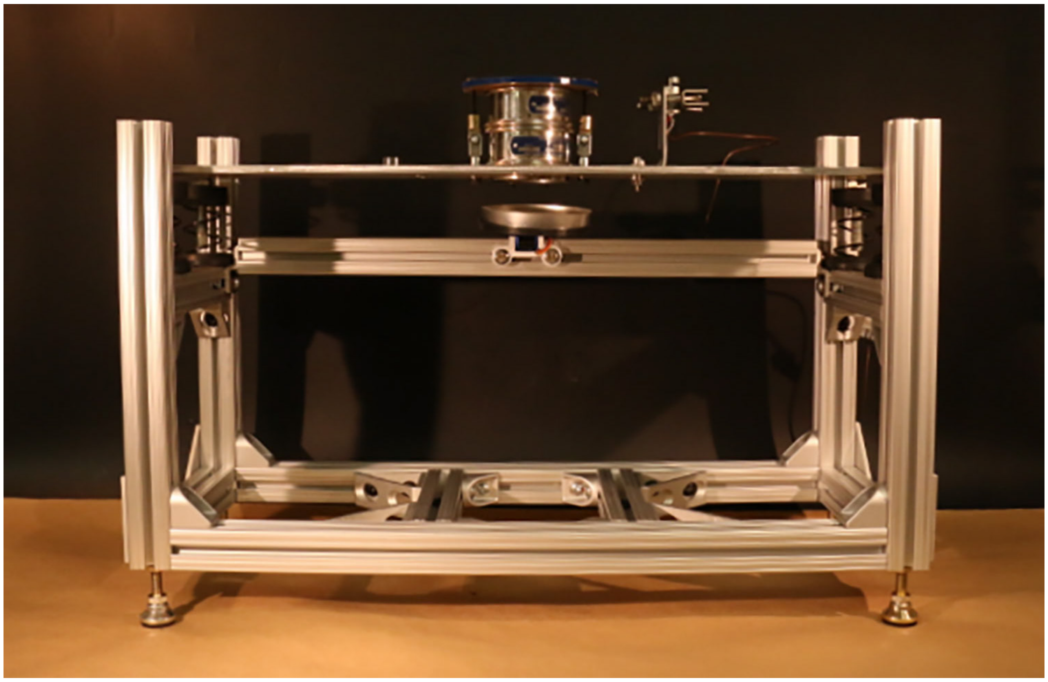

Figure 2.—Deposition subsystem (shown outside glovebox).

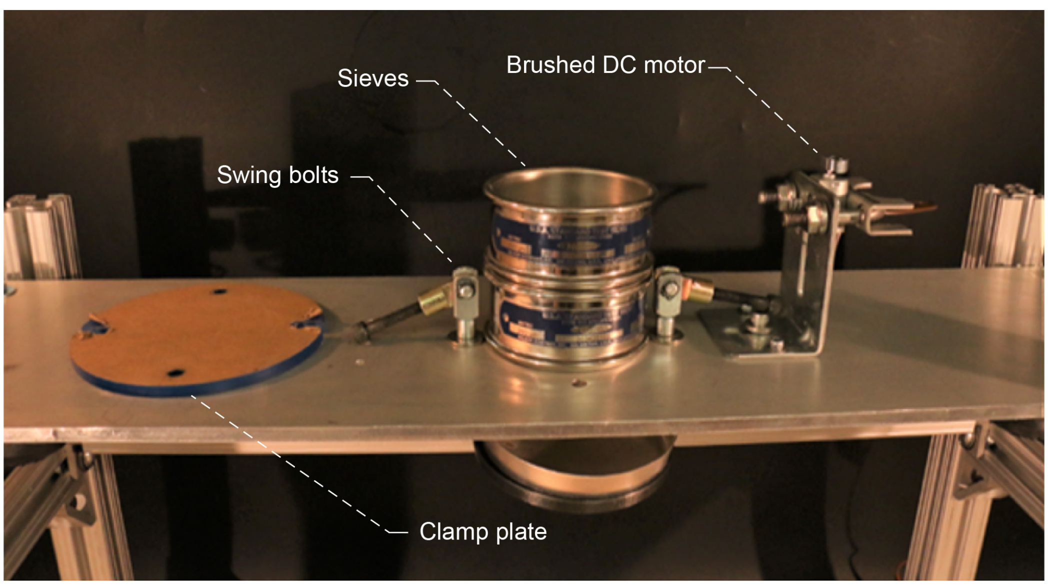

Figure 3.—Vibration plate top view showing sieves, swing bolts, motor, and sieve clamp plate. Direct current, DC.

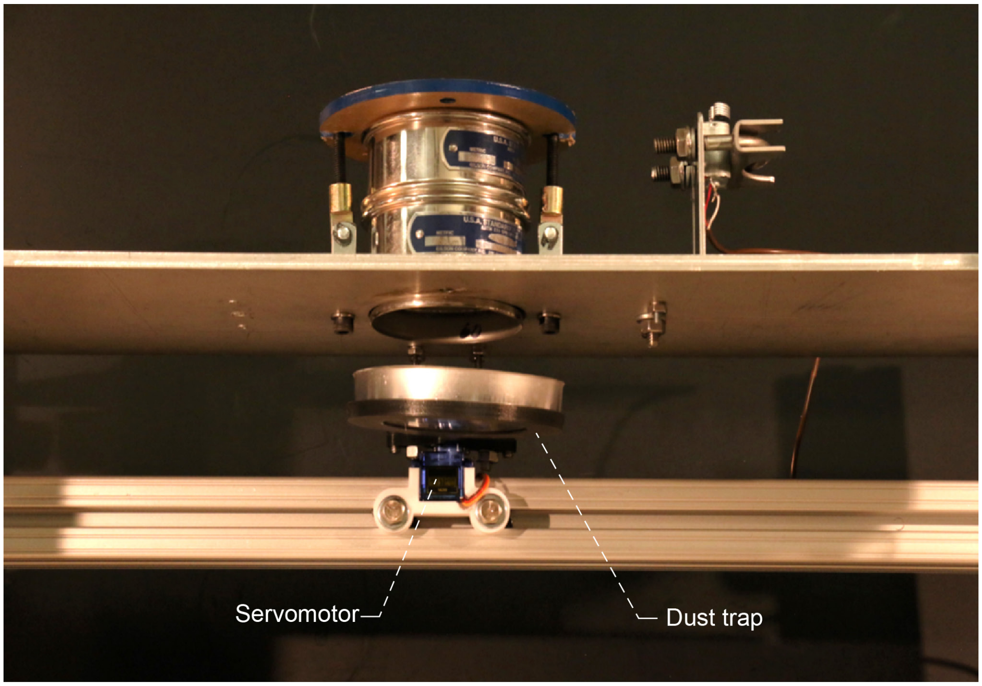

Figure 4.—Dust trap.

The final component that can be mounted on the vibration plate is an optional inertial measurement unit (IMU) or accelerometer. A 3-axis sensor is recommended for capturing all motion data. This device measures the amplitude and frequencies of the vibration plate during agitation. These measured values can be used as a feedback signal for closed-loop control of the vibration of the plate. A fast Fourier transform can be done on the vibration signals to find their frequency temporally. Frequency response was explored initially, and it was found that characterizing the harmonic frequencies of the system with known masses of simulants in the sieves was suitable for the initial characterization. (This process is explained in the verification section of this paper).

To further increase the accuracy of the deposition subsystem, a dust trap was added under the vibration plate beneath the openings of the sieves. The dust trap is mounted to a rigid point on the deposition system frame to eliminate any unwanted mass on the vibration plate and protect the servomotor from the vibrations. This dust trap consists of a servomotor connected to a lightweight arm that holds an aluminum cup (Figure 4). The cup catches any simulant that leaves the sieves before the eccentric mass motor is operating at the desired speed (e.g., ramping up from rest). The dust trap actuates only when the deposition is at steady state. Its actuation is quick enough to allow for immediate deposition on the target surface but slow enough to mitigate disturbance of the deposition column.

Transfer Subsystem

The transfer subsystem's function is to accurately position the target surface beneath either the deposition subsystem or the imaging subsystem in a repeatable fashion. A secondary role of the transfer subsystem is to help automate the deposition and characterization process and produce accurate and repeatable movements. The system consists of a pair of parallel rails that support a transfer carriage. On that carriage sits a spin plate where the target surface is installed. Both the rail and spin plate components are motorized using two National Electrical Manufacturers Association (NEMA) 23 stepper motors connected to chain drives (Figure 5). All components of the transfer system are made of vacuum-compatible materials, such as aluminum, 304 stainless steel, and 18-8 stainless steel.

To increase the dust tolerance of the system, the V-track rails and chain drives were baselined. The V-track rails are oriented with their apex facing up to shed as much of the dust as possible and reduce accumulation. V-groove wheels with sealed bearings were installed on the transfer carriage to mate with the rails. The chain drive connecting the transfer carriage to the NEMA 23 motor was baselined for its favorable dust tolerance versus a ball screw and lead screw architecture. Although not depicted, the transfer carriage can be modified to have a second set of V-track rails that lie perpendicularly to the original set. The stepper motors mounted on the transfer carriage can then be used to actuate a second transfer carriage, giving the system the ability to deposit with an X-Y scheme, much like three-dimensional (3D) printers use.

The last component of the transfer subsystem is the spin plate. This plate sits on the transfer carriage and is driven by a chain drive connected to a NEMA 23 stepper motor, which also sits on the carriage (Figure 6). This plate has positioning features for repeatable alignment of target surfaces and fixtures. One such fixture that is often used during dust deposition is a dust mask. The dust mask covers and protects sensitive areas of the target surface while still permitting dust deposition in specific areas of interest. It is often a plate with a hole or opening in the area(s) of interest. For example, if a 2-309 O-ring was the test specimen on which dust was being deposited, its dust mask would be any plate with an outer diameter larger than the full target surface with a 2.11-cm-diameter hole in the center for the O-ring to sit in (Figure 7). This protects the other regions of the target surfaces from collecting dust.

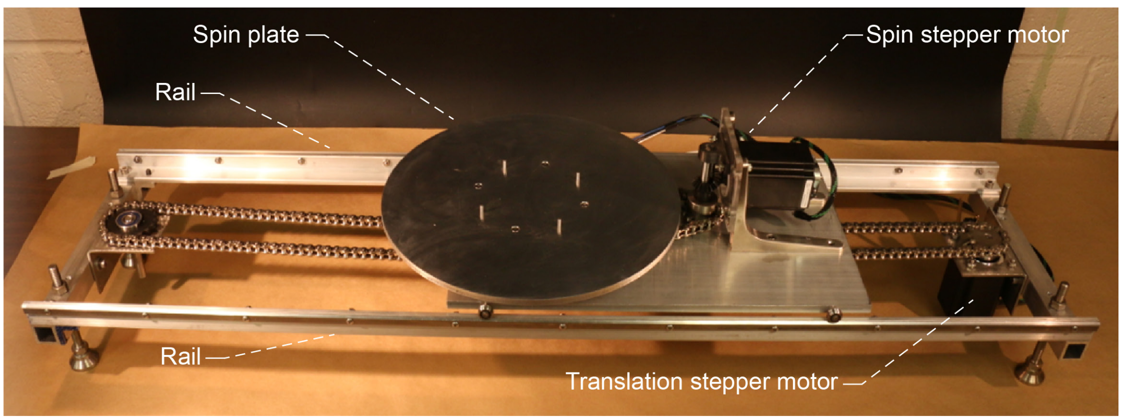

Figure 5.—Transfer subsystem (shown outside glovebox).

Figure 6.—Spin plate installed on carriage on transfer rails.

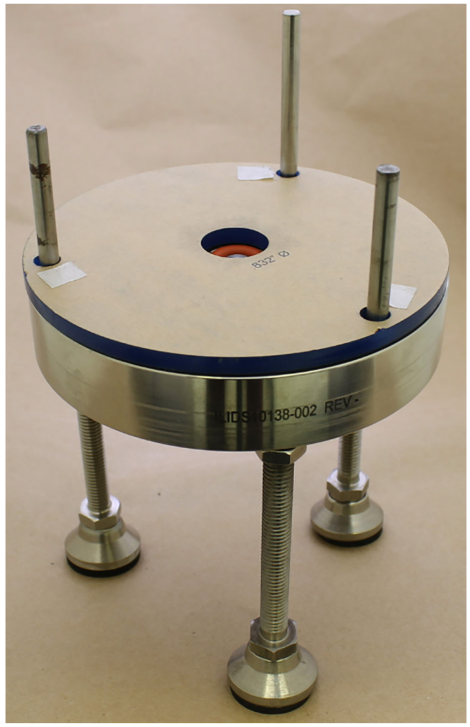

Figure 7.—Dust mask for 2-309 O-ring.

Imaging Subsystem

The imaging subsystem captures micrographs at various locations on the sample surface while both are still inside the dry-air environment of the glovebox. A stereo microscope (Motic SMZ–171 model) capable of magnification levels from 7.5× to 100× was coupled with a 10-MP microscope camera (Moticam 10+ model) to inspect the sample surfaces and obtain the desired micrographs. To protect the imaging subsystem from dust, a custom enclosure and stand were built around it (Figure 8). This enclosure surrounds the entire microscope and camera while still allowing room for the microscope to be moved up and down to adjust its focal distance for image stacking. The bottom face of the enclosure features an optically clear 5-cm-diameter quartz disc below the objective lens to provide a clear sightline to the target surface. To illuminate the target surface, an 80-LED, 6,400-K ring light was mounted around the objective lens of the microscope. Finally, lens caps were added to the eyepieces of the microscope to prevent unwanted ambient lighting from entering the camera's sensor during imaging.

To obtain an image with a depth of field larger than the microscope's lenses could offer (e.g., the curved surface of an O-ring), a z-stacking capability was implemented. This was accomplished by attaching a NEMA 23 stepper motor to the focus stage of the microscope. To complement this capability and improve the automation of the testing, the imaging system was tied to the transfer system's spin plate to allow rotation of the target surface. This rotation feature can be used when images of several locations of a target surface are desired. Once the imaging routine finishes an image stack, the spin plate can rotate to a new prescribed area and another stack can be captured. This is especially useful when testing deposition uniformity. All the stepper motors were controlled with the same software as the rest of the system on a control box outside of the glovebox.

The microscope, camera, and motor are used to capture several images of the target surface at varying focal distances. This creates an image stack, which is postprocessed using ImageJ software (Ref. 15) through the Fiji package (Ref. 16). The Stack Focuser plugin (Ref. 17) is used in conjunction with the base Fiji package to perform the image analysis. To mitigate any shifting or misalignment in images, individual image stacks are registered, or aligned, to each other using the Linear Stack Alignment with SIFT (scale-invariant feature transform) plugin (Ref. 18). The Stack Focuser plugin is then used to create a single image with an extended depth of field from the aligned stack. The Trainable Weka Segmentation plugin (Ref. 19) is then used to segment the focused image. This is a machine learning plugin that is trained to separate the particles from the background using a training dataset that the user creates manually from dusted images. This dataset is used to create a classifier algorithm that can accurately segment additional images with the same substrate. The Trainable Weka Segmentation plugin is used to output a probability map of the image. A threshold is applied to a probability map and input into the Analyze Particles tool in Fiji, where the tool counts particles based on the intensity of the pixels. This tool outputs many potentially helpful metrics, particularly the percent area, which is used to calculate uniformity and deposition density. This entire process is summarized in Figure 9. An example of an image the algorithm would analyze is shown in Figure 10. To obtain sufficient image quality and confidence in the data, 100 pixels was set as the minimum resolution with which a single particle could be imaged. This resolution then implies that the smallest diameter particle the current system can accurately identify is 8 µm, which is less than the 10-µm requirement.

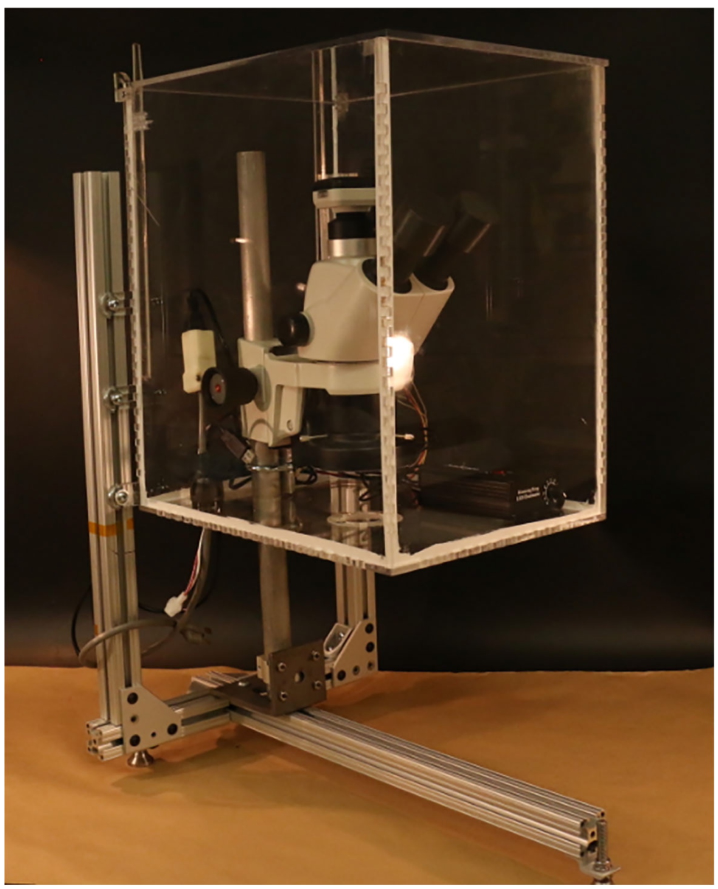

Figure 8.—Imaging subsystem (shown outside glovebox).

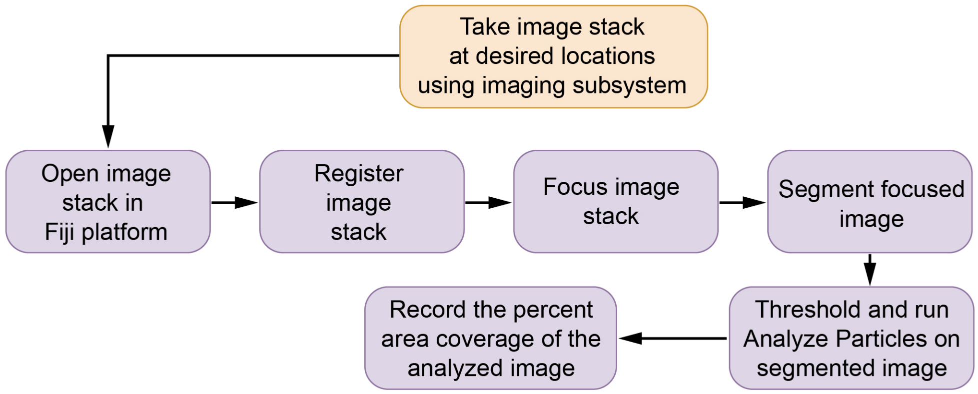

Figure 9.—Imaging Concept of Operations (CONOPS).

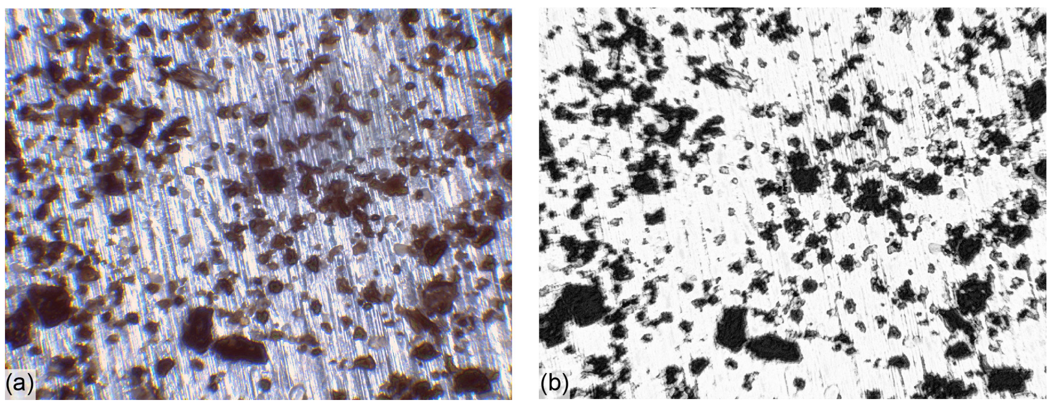

Figure 10.—JSC–1A lunar dust simulant on aluminum tray at 50× magnification. (a) Focused image. (b) Segmented image.

Peripheral Components

This section describes other components that were found to be particularly useful during the design of the UDDS. A bright yellow light was very useful to backlight the simulant when taking video of the deposition process. The light also helped the operator visually evaluate the uniformity and rate of the deposition in situ and in real time, allowing a test to be aborted early if an anomaly was detected. A designated waste container within the glovebox was found to be valuable to dispose of any wipes, test samples, or debris without having to open the transfer chamber of the glovebox during testing.

For the measurement of the RH and the temperature, a Vaisala DMT340 sensor capable of reading RH from 0 to 70 percent (±0.004 percent + 20 percent of reading) and temperatures from 0 to 80 °C (±0.2 °C) was used. The sensor's probe was mounted inside the glovebox and was biased toward the upper middle of the back wall. Another instrument that facilitated testing was an Ohaus EX225/AD electronic balance, also located inside the glovebox. This device not only met the weighing requirements (220-g capacity with 0.01-mg readability) but was compact enough to fit inside the glovebox. This capability improved the accuracy of the mass readings because the measurements could be taken in a dry environment where the samples would not absorb any atmospheric moisture.

Simulant Preparation

Lunar regolith simulant is by nature a collection of particles of dissimilar size, mineralogy, and shape. The manufacturers of these simulants take extreme care in generating batches that have constituents and PSDs that match various Apollo mission samples or data from orbiters. However, technology developers sometimes desire the ability to isolate certain PSDs. Finer PSDs may be valuable for evaluating the performance of solar panels or radiator panels because the smaller particles tend to adhere more aggressively due to electrostatic charging. Larger particles may be useful for life-testing mechanisms, such as latches and rotary joints for abrasion resistance. With the need to test simulants in a uniform and repeatable way, a technique was developed to preprocess bulk simulants in preparation for testing.

The simulant preparation process consists of four steps: sieving, drying, rolling, and storing. In the first step of the process, bulk simulant is gathered in sufficient amounts and is then transferred to a sieve stack in a mechanical tapping sieve or shaker. The guidelines of American Society for Testing and Materials (ASTM) standard D6913 are then followed to achieve the desired PSD (Ref. 20).

After the simulant has gone through the sieving process, it is spread over a large metal tray for desiccation. The tray is then placed in a vented oven that has been preheated to 110 °C and left there for 12 to 16 hr. This desiccation technique is based on ASTM standard D2216 (Ref. 21). One suggestion presented in the standard that was found to be particularly useful was the "paper curl" test. This test consists of opening the drying oven and placing a dry, torn piece of paper on top of the sieved simulants. If the paper curls, this indicates there is still moisture in the sample. The drying process continues until the paper strips no longer curl.

The third step in the process is the rolling of the sieved and desiccated simulant. This is done by placing the simulant into a sturdy, sealed, cylindrical container and placing it on a laboratory roller for 30 min. This allows the selected PSDs to recombine into a more homogenous distribution within the container. Note that the samples tend to separate over time if left on a shelf. To address this issue, the sample containers should be rolled again before use (even if just by hand) to ensure homogeneity. Experience shows batching the larger desiccated batch into smaller portions in separate containers helps ensure that each test sample is insulated from passive separation due to settling. This batching process also helps expedite test flows by making separate, smaller containers of simulant available for every test.

The final step is storing the prepared simulant. The recommended approach is to place the prepared simulant in a sealed container, such as a glass laboratory jar, in an atmosphere that is as dry as possible. For the UDDS, this is accomplished by opening and closing the containers in the glovebox with its dry purged atmosphere. The mass of each container is monitored by weighing it prior to storage and then again before use to evaluate if any moisture has been absorbed. To further ensure no moisture intrusion, the containers are placed into the dry environment of the glovebox for storage. These procedures help ensure that the simulant behaves in a predictable manner from test to test, thereby producing the best results.

Test Procedure

This section describes the process for a typical experiment involving deposition onto a target surface. The test procedure is separated into three phases: pretesting, testing, and posttesting. Before conducting any testing, the simulant is prepared by following the process described in the previous section.

Pretesting

The pretesting phase begins by ensuring that all appropriate safety controls are in place, particularly appropriate respiratory protection. All fixtures and equipment are cleaned with isopropyl alcohol, including simulant containers, target surfaces, weighing dishes, tweezers, and gloves. With the inner door of the transfer chamber of the glovebox closed, any equipment required for the test is placed inside the chamber before closing its outer door. The inner door of the transfer chamber is then opened to access the equipment for the test. The purge valve of the dry air system is opened to purge the atmosphere of the glovebox until it reaches less than 1 percent RH. The inner door of the transfer chamber is then closed, and the temperature and atmospheric pressure of the lab are recorded. Finally, the subsystems of the UDDS (deposition, transfer, and imaging) are visually inspected and powered on, and dry runs are performed to ensure that they are functioning properly before the simulant is loaded.

Testing

After the subsystems have been checked out, the testing phase can begin. The first step is to load the simulant into the sieves of the deposition system. After cleaning and brushing the sieves, the lower sieve is left in place in the vibration plate, and the upper sieve is placed on a weighing dish. The simulant container is then selected and rolled at least 10 full rotations about its major axis. It is then opened, and its contents are deposited onto the center of the upper sieve. The upper sieve and weighing dish are then lifted together and gently swirled in a circular motion along the plane of the sieve mesh one time to ensure the simulant completely covers the mesh surface of the upper sieve. Finally, the upper sieve is stacked on top of the lower sieve on the vibration plate, and the sieve clamping plate is installed.

After the simulant has been loaded, the target surface is positioned on the carriage of the transfer system and is clocked in a known and repeatable fashion. This is particularly important for target surfaces that are larger than the 7.63-cm-diameter deposition area; these larger surfaces must be rotated to deposit simulant on the entire surface. For example, if the target surface is a 30-cm-diameter seal, it will be mounted on the transfer assembly so it can be repeatably rotated and aligned for every test. One way this is done is by having the fixture interface with alignment pins on the spin plate of the transfer carriage. This feature, combined with the precision of the stepper motors, enables exact manipulation of the large target surface during the deposition, ensuring the entire area receives a uniform deposition.

The actual test now begins by executing a homing routine for the transfer systems, followed by a translation to the area under the deposition system. The spin stage is then triggered to start rotating the target surface. The deposition system is activated, and the routine runs for the prescribed amount of time. The translation system then moves the carriage under the imaging system, where the microscope software is remotely triggered along with the rotation stage to image various areas of the target surface. After the deposition and imaging are complete, the fixture is moved to the home position, where the target surface can be removed and weighed if desired. As noted previously, the target surface is typically weighed inside the glovebox to prevent the deposited simulant from absorbing atmospheric moisture from the laboratory. In cases where the sample is too large or too heavy to weigh, the image analysis is critical to evaluating the deposition density (explained in greater detail in the validation testing section). The test sample can now be removed from the glovebox through the transfer chamber for subsequent performance evaluations (e.g., leak tests on seals, transmissibility testing of glasses, and thermal testing of radiators).

Posttesting

The posttesting phase begins with the unloading of the simulant from the deposition system's sieves. The excitation frequency for the vibration plate is dependent on the vibrated mass. If there has been a significant change in weight of the simulant in the sieve, it is recommended that a new container-prepared simulant be used. When changing the simulant, the first step is to transfer all remaining original simulant in the sieves to a "spent" container. (Note: It is not economically practical to discard simulant; as long as it is recharacterized it may be used in the future). The sieves are then brushed to liberate any stuck particles. Next, the glovebox is left to sit idle for a minimum of 1 hr to allow all the particles suspended in the air to settle. Surfaces within the glovebox are wiped clean using wipes with isopropyl alcohol, taking care not to scratch glass surfaces where simulant may have adhered (e.g., optical glass and the glovebox window). To further clean the glovebox, a vacuum cleaner with an appropriate high-efficiency particulate air (HEPA) filter may be used. The posttesting phase is now complete. The entire testing flow is described pictorially in Figure 11.

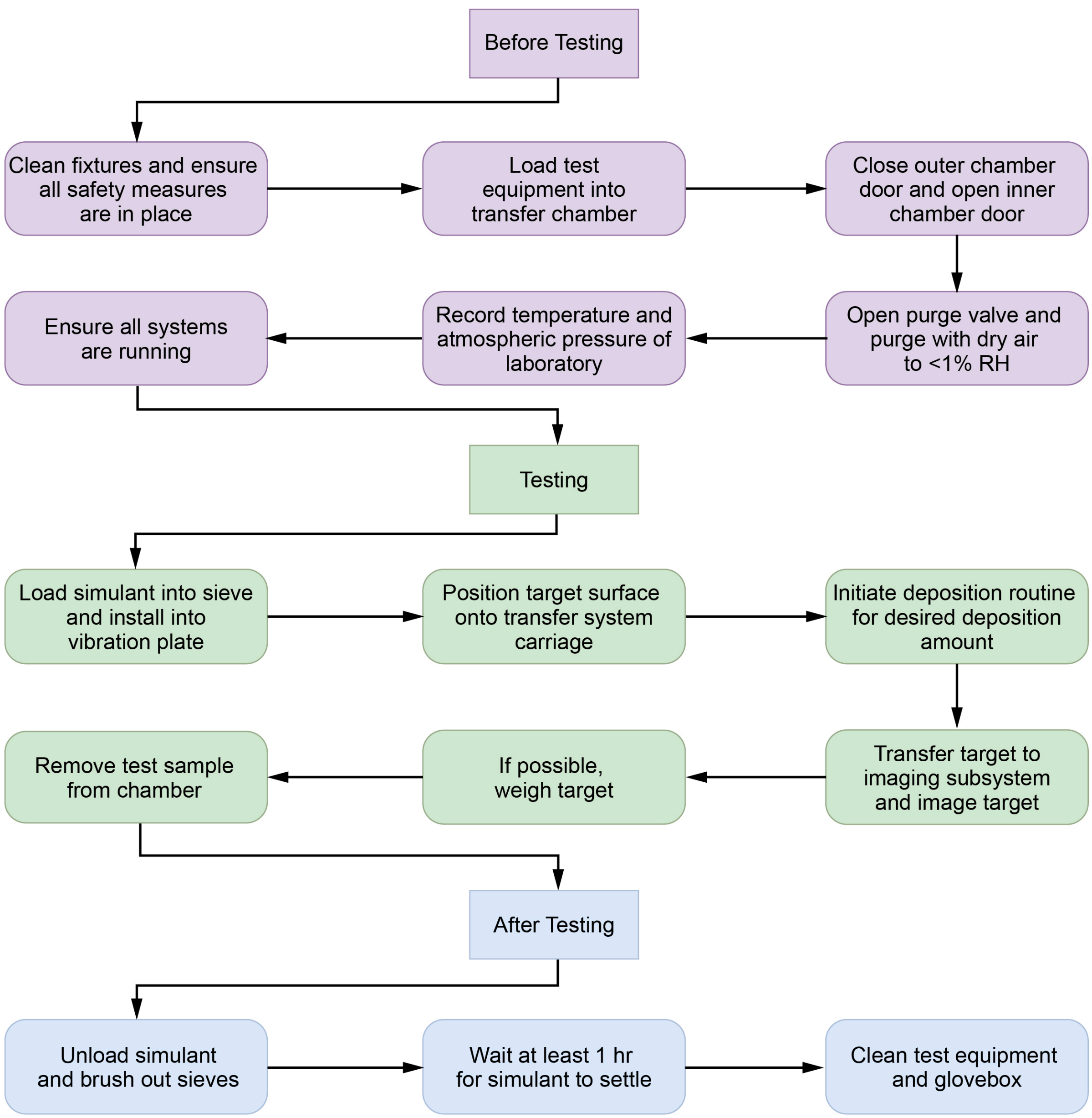

Figure 11.—Flow chart of typical test.

Validation and Verification Testing

Tests were performed to verify and validate that the UDDS can deposit lunar dust simulant in a uniform, accurate, and repeatable manner. The verification tests confirmed that the system can deposit simulant in a controllable fashion and were used to characterize the modal and electrical characteristics of the system. The validation testing then tuned the system to obtain desired deposition rates and densities.

Verification Testing

The main objectives of this series of tests were to find the harmonic frequencies of the deposition system and to determine the ideal mass of simulant that should be loaded into the sieves. It was discovered that the test results were dependent on the specific motor and supplied voltage used in the system. There were three test series, each with a different mass of simulant in the sieves (20, 25, and 50 g). For every trial in the series, a new batch of desiccated JSC–1A simulant (<250 µm PSD) was loaded into the sieves and vibrated for 10 s. The target surface for deposition was an aluminum weighing tray placed below a mask plate. The mask plate had a 5-cm-diameter hole cut out in its center, which allowed for isolation of the central deposition area (Figure 12). The mass of simulant deposited on the tray was recorded for a range of duty cycles, where duty cycle is defined as the pulse width sent to the direct-current (DC) motor. For example, a 50-percent duty cycle meant that for a given time pulse, the voltage of the motors was set to full voltage for half of that pulse.

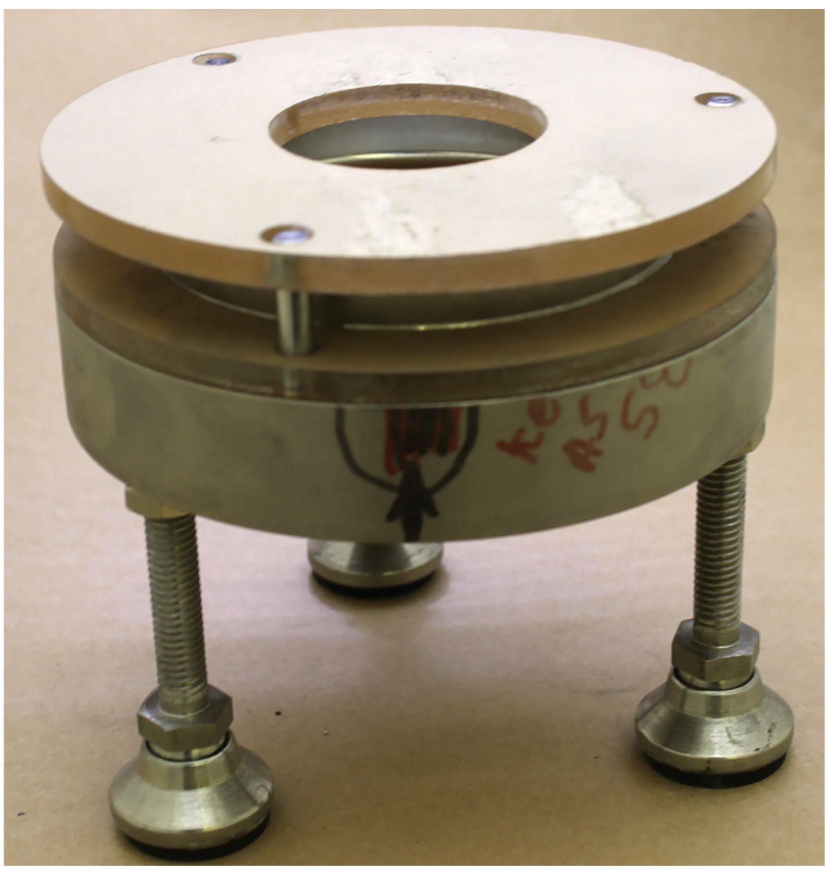

Figure 12.—Test fixture for verification testing: Aluminum weighing tray below mask with 5-cm-diameter opening.

The first step in this testing series was to find the “dead zone” of the 3-V DC motor, the lower range of voltages at which the motor would not have enough power to rotate its mass. The duty cycle for the motor was increased gradually until the motor’s mass began to move slightly. Once that value was found (31 percent for the motor used), it was hard coded into the deposition routine as the starting duty cycle. Each trial in the three mass-series then followed the same sequence of steps. First, a target duty cycle was selected by starting at a value 4 percent above the dead zone for the initial trial. This was then increased by 2.5 percent for each subsequent trial. The motor was powered up to the dead zone duty cycle, steadily ramped up to the target duty cycle, and then held there for 5 s to allow the system to reach steady state. After the 5 s, the dust trap was opened, and the system deposited simulant on the tray for 10 s. After the 10 s, the dust trap immediately closed to prevent any continued deposition from reaching the target surface. The mass deposited on the tray was then weighed and recorded, the systems were reset, and the next trial was run. The same procedure was used for all three different masses of simulant in the sieves. The results of these trials are shown in Figure 13.

The harmonic frequency of the vibration plate was found whenever the deposited mass values greatly increased. This can be seen in Figure 13. During harmonic depositions, the flow of simulant out of the sieves was heavy and difficult to control. As noted from the figure, the harmonic phenomenon started to occur at a duty cycle of 59 percent for 20 g of simulant and increased slightly as more simulant was added to the sieve. This agrees with theory, as a larger mass requires more energy to reach the same level of excitation. The optimal duty cycle selected was 53 percent, as this represented an output where all three curves had moderate slopes before reaching the first harmonic frequency (Figure 13). The optimal sieve simulant mass selected was 25 g, as it showed measurable levels of deposition while displaying a linear correlation between deposited mass and duty cycle.

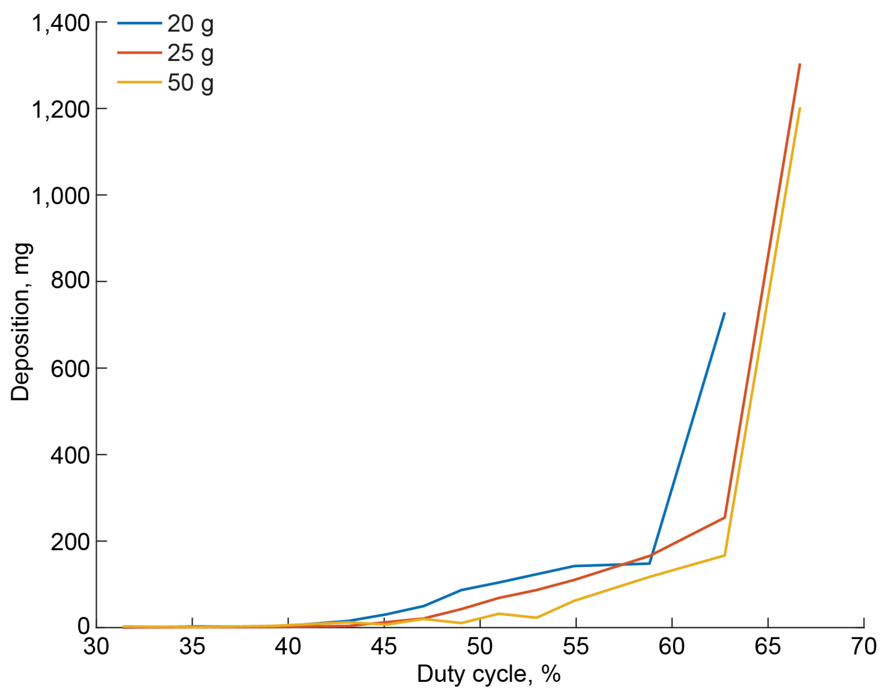

Figure 13.—Deposited mass (mg) versus motor duty cycle (percent) (10-s depositions) for various sieve simulant masses.

Validation Testing

Once the system was characterized and the desired duty cycle and sieve simulant mass were identified, testing was conducted to tune the system for desired deposition amounts. Two series of tests were conducted to validate the system's performance. The first series evaluated deposition accuracy by varying deposition time and the number of deposition runs to correlate the time rate of deposition to deposited mass. The second series of tests evaluated deposition uniformity by relating the percent area coverage as measured by the imaging system to the actual mass deposited.

Deposition time testing quantified the accuracy and precision of the system. As noted earlier, the 53-percent duty cycle was selected along with a 25-g mass of JSC–1A simulant (<250 μm PSD) in the sieve. The deposition time was the independent variable and was evaluated at 10, 20, and 30 s. The target surface for these tests was again an aluminum weighing tray installed under a mask with a 5-cm-diameter opening. The test flow was similar to the process described for the verification testing with the exception of deposition time. Repeats at every deposition time interval gave precision data, and the incremented time yielded accuracy data (a specific deposition mass). The results of this testing can be seen in Figure 14. For each time interval, the amount of simulant deposited varied, and the ranges obtained overlapped with each other. The standard deviations (SDs) of the 10-, 20-, and 30-s trials were 18, 17, and 24 mg, respectively, showing a moderate level of precision. Figure 14 also shows a weak correlation between the deposition time and mass deposited (accuracy), meaning that there is some difficulty in hitting a prescribed deposition density in a single deposition.

The second series of validation tests for the deposition system differed from the first series in the target (time versus mass) and process. In the first series, the process was a single deposition for a given time. In this next series of tests, multiple depositions were run to reach a target final mass. Four target masses were selected for the characterization tests: 5, 7.5, 10, and 12.5 mg. Three or four repeat tests were performed for each target value. The SDs were 0.613, 0.213, 0.327, and 0.234 mg for the 5-, 7.5-, 10- and 12.5-mg targets, respectively (Figure 15). This process works well for surfaces that can be weighed

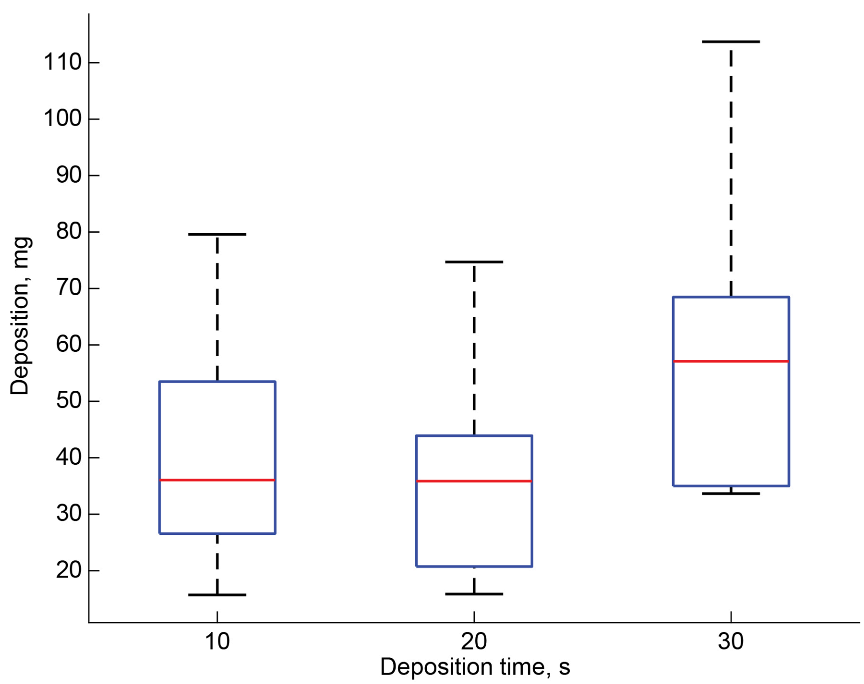

Figure 14.—Accuracy testing: Box-and-whisker plot of deposited mass trials for three deposition times, single deposition run.

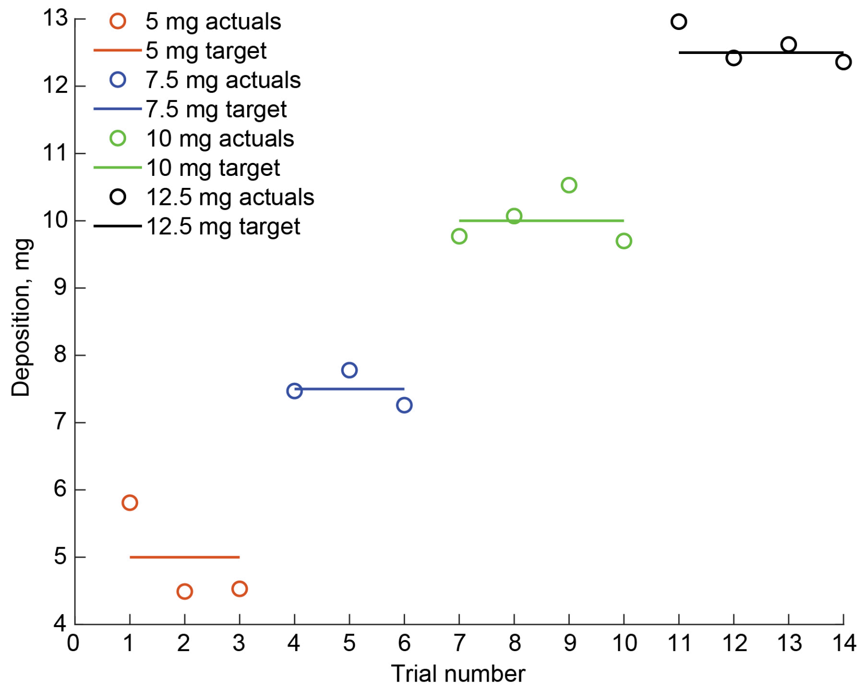

Figure 15.—Accuracy testing: Deposited mass trials with multiple deposition runs.

(i.e., small test articles such as O-rings). However, it is not suited for larger test articles. Therefore, the imaging system was used to develop an analysis technique that could work for targets of all sizes.

The aim of the third series of validation tests was to obtain a correlation between the percent coverage value that the machine learning algorithm produced after analyzing dust deposition images and the actual mass of deposited simulant. To check uniformity, imaging data was captured during the trials performed for the first series of validation tests. After every 10-, 20-, and 30-s deposition trial, the weighing tray was moved under the imaging system. The surface of the weighing tray was divided into five subsections, one in each quadrant and one in the center of the deposition area. A set of images was taken for each subsection and combined into one high-resolution, high-depth-of-field image. The stacked image was then entered into a machine learning algorithm trained to recognize simulant particles, count them, and calculate the percent of the surface area covered by the simulant. The percent coverages for the five subsections were then averaged for each trial. The CV of these percent coverage values was calculated for each trial, and the CV values were plotted against the deposition times as shown in Figure 16. The low CV values indicate that there is a very uniform deposition throughout the trials independent of deposition time.

Next, the correlation for deposited mass versus percent coverage was evaluated. An R^2 value of 0.93 was calculated for the correlation between the percent coverage and the actual mass of simulant on a surface (Figure 17). This provided a high level of confidence in the ability to predict deposition density, or how much simulant was deposited on a surface, using the imaging system to measure percent coverage. This capability is extremely important to have, as test articles are often too large or too heavy to be accurately weighed during dust testing. Furthermore, the SD of percent coverage for all trials was always less than 6 percent with a mean of 3.5 percent across the dataset. The deposition area for the characterization tests was a 5-cm-diameter circle (20.3-cm^2 area). Regarding deposition densities, the average SDs for 10-, 20-, and 30-s depositions were 0.909, 0.889, and 1.213 mg/cm^2, respectively, all low enough to satisfy the ±1.5-mg/cm^2 requirement. The significance of a uniform deposition comes into play when testing dust mitigation technologies, and the excellent uniformity of the dust distribution observed will produce more meaningful testing results.

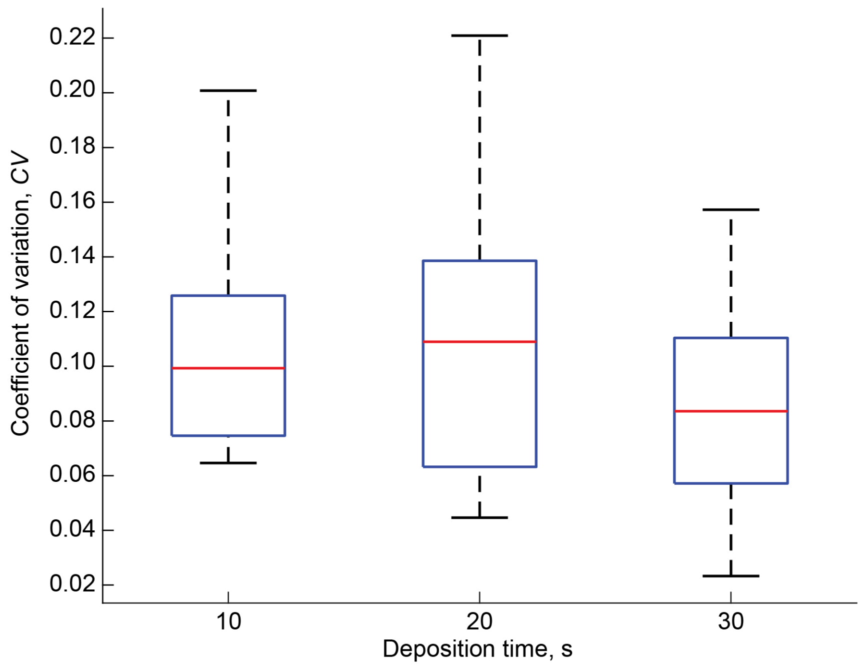

Figure 16.—Box-and-whisker plot showing coefficient of variation (*CV*) for various percent coverage of trials for different deposition times.

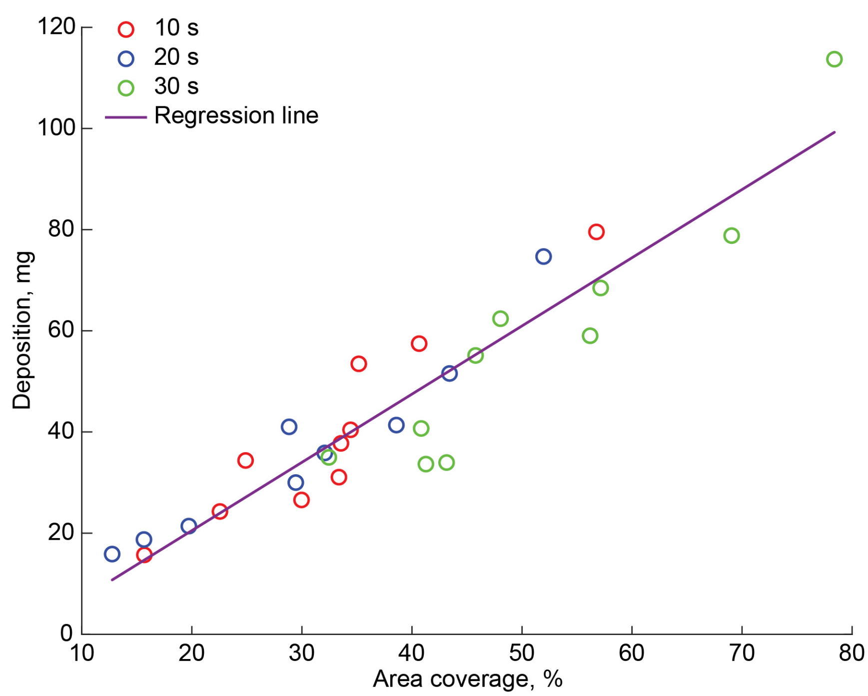

Figure 17.—Imaging precision results, mass versus percent coverage; regression line calculation is $y = 1.348623 \cdot x + 6.458526$; coefficient of determination (R^2) value is 0.93.

Concluding Remarks

The Uniform Dust Deposition System (UDDS) was developed at the NASA Glenn Research Center to provide repeatable, uniform, and automated deposition of simulants on surfaces of interest for dust mitigation testing. The system is capable of depositing simulants on test articles up to 60 cm in diameter and 15 cm high in a dry air environment with less than 1 percent relative humidity while keeping users safe from aerosolized dust. The automation of the system allows for high testing throughput while not sacrificing test quality and allows the user to reduce data in parallel. The additional development of a simulant preparation technique complements the repeatability of the deposition physics during testing. The system includes an imaging subsystem that leverages the power of machine learning to count simulant particles and measure their size, thereby allowing for accurate predictions of surface deposition densities (coefficient of determination $R^2 = 0.93$) from images alone. The coverage of dust on a surface was shown to be uniform (coefficient of variation $CV < 0.11$) allowing developers to accurately evaluate the performance of their technology with a prescribed amount of lunar simulant, information that can be used to develop and refine models. The accuracy of the system is currently less than desired for a single deposition run, with a standard deviation (SD) ranging from 18 to 24 mg, or 0.839 to 1.184 mg/cm^2, for a 5-cm-diameter area. However, the accuracy can be improved by performing multiple deposition runs to build dust to a desired level. Testing has shown that a SD of 0.2 to 0.6 mg, or 0.076 to 0.227 mg/cm^2, can be achieved for a 5-cm-diameter area using this technique.

Forward work has been planned to improve the single-deposition accuracy of the system. The ultimate aim is to develop a system that can then be duplicated and used inside a thermal vacuum chamber that is currently being procured. However, the existing UDDS and its potential expanded capabilities are expected to be valuable tools for technology developers and scientists in the development of dust mitigation technologies.

References

1. Executive Office of the President: Reinvigorating America’s Human Space Exploration Program. Space Policy Directive–1 of December 11, 2017, Federal Register, vol. 82, no. 239, 2017, pp. 59501–59502.
2. Crotts, Arlin: The New Moon: Water, Exploration, and Future Habitation. Cambridge University Press, New York, NY, 2014, p. 334.
3. Heiken, Grant H.; Vaniman, David T.; and French, Bevan M., eds.: Lunar Sourcebook. Cambridge University Press, New York, NY, 1991, pp. 285–356.
4. Pieters, Carle M., et al.: Space Weathering on Airless Bodies: Resolving a Mystery With Lunar Samples. Meteorit. Planet Sci., vol. 35, no. 5, 2000, pp. 1101–1107.
5. Stubbs, Timothy J., et al.: Lunar Surface Charging: A Global Perspective Using Lunar Prospector Data. Workshop on Dust in Planetary Systems Proceedings, vol. 643, 2005, pp. 181–184.
6. Hood, N., et al.: Laboratory Measurements of Size Distribution of Electrostatically Lofted Dust. Icarus, vol. 371, no. 114684, 2022.
7. Buhler, C.R., et al.: Test Method for In Situ Electrostatic Characterization of Lunar Dust. IEEEAC Paper 1666, version 2, 2007.
8. Belden, Lacy, et al.: Design of Equipment for Lunar Dust Removal. NASA CR–190014, 1991. https://ntrs.nasa.gov
9. Winterhalter, Daniel, et al.: Lunar Dust and Its Impact on Human Exploration: A NASA Engineering and Safety Center (NESC) Workshop. NASA/TM—2020-5008219 (NESC–RP–19–01469), 2020. https://ntrs.nasa.gov

10. John, Kristen Kathleen; and Rogers, Charles E.: Classifications and Requirements for Testing Systems and Hardware to be Exposed to Dust in Planetary Environments. NASA–STD–1008, 2021. https://ntrs.nasa.gov
11. Oravec, H.A.; and Daniels, C.C.: Leak Rate Performance of Silicone Elastomer O-Rings Contaminated With JSC–1A Lunar Regolith Simulant. Earth and Space 2014, St. Louis, MO, 2014.
12. Kawamoto, Hiroyuki: Electrostatic Cleaning Equipment for Dust Removal From Soiled Solar Panels. J. Electrostat., vol. 98, 2019, pp. 11–16.
13. Gaier, James R.; and Sechkar, Edward A.: Lunar Simulation in the Lunar Dust Adhesion Bell Jar. NASA/TM—2007-214704 (AIAA 2007–0963), 2007. https://ntrs.nasa.gov
14. Yuan, Jingjie, et al.: Experimental Investigations on the Roles of Moisture in Coal Dust Explosion. J. Taiwan Inst. Chem. Eng., vol. 45, no. 5, 2014, pp. 2325–2333.
15. Schindelin, J., et al.: The ImageJ Ecosystem: An Open Platform for Biomedical Image Analysis. Mol. Reprod. Dev., vol. 82, nos. 7 and 8, 2015, pp. 518–529.
16. Schindelin, J., et al.: Fiji: An Open-Source Platform for Biological-Image Analysis. Nat. Methods, vol. 9, no. 7, 2012, pp. 676–682.
17. Umorin, Mikhail: Stack Focuser. https://imagej.nih.gov/ij/plugins/download/Stack_Focuser_.java. Accessed Jan. 11, 2022.
18. Lowe, David G.: Distinctive Image Features From Scale-Invariant Keypoints. Int. J. Comput. Vis., vol. 60, no. 2, 2004, pp. 91–110.
19. Arganda-Carreras, I., et al.: Trainable Weka Segmentation: A Machine Learning Tool for Microscopy Pixel Classification. Bioinformatics, vol. 33, no. 15, 2017, pp. 2424–2426.
20. ASTM D6913/D6913M–17: Standard Test Methods for Particle-Size Distribution (Gradation) of Soils Using Sieve Analysis. ASTM International, West Conshohocken, PA, 2004.
21. ASTM D2216–05: Standard Test Methods for Laboratory Determination of Water (Moisture) Content of Soil and Rock by Mass. ASTM International, West Conshohocken, PA, 2010.